[o]Ordered arrays of polymeric nanopores by using inverse nanostructured PTFE surfaces

Jaime Martín[1], Marisol Martín-González[1,*], Adolfo del Campo[2], Julián J. Reinosa[2], and José Francisco Fernández[2]

[1] Instituto de Microelectrónica de Madrid (CNM-CSIC), Isaac Newton 8, PTM, E-28760 Tres Cantos, Madrid, Spain
[2] Instituto de Cerámica y Vidrio (ICV-CSIC), Kelsen 5, 28049 Cantoblanco, Madrid, Spain

E-mail: marisol@imm.cnm.csic.es

Abstract. We present a simple, efficient, and high-throughput methodology for the fabrication of ordered nanoporouses polymeric surfaces with areas in the range of cm^2. The procedure is based on a two-stage replication of a master nanostructured pattern. The process starts with the preparation of an ordered array of PTFE (poly(tetrafluorethylene)), PTFE) free-standing nanopillars by wetting self-ordered porous Anodic Aluminum Oxide (AAO) templates with molten PTFE. The nanopillars are 120 nm in diameter and approximately 350 nm in length, while the array extends over cm^2. The PTFE nanostructuration process induces a surface hydrocarbonation of the nanopillars, as revealed by confocal Raman microscopy/spectroscopy, which enhances the wettability of the originally hydrophobic material and facilitates its subsequent use as an inverse pattern. Thus, the PTFE nanostructure is then used as a negative master for the fabrication of macroscopic hexagonal arrays of nanopores composed of biocompatible poly(vinylalcohol) (PVA). In this particular case, the nanopores are 130-140 nm in diameter and the interpore distance is around 430 nm. Features of such characteristic dimensions are known to be well recognizable by the living cells. Moreover, the inverse mold is not destroyed in the pore array demoulding process and can be reused again for a new pore array fabrication. Therefore, the developed method allows the high throughput production of cm^2-scale biocompatible nanopores surfaces that could be interesting as two-dimensional scaffolds for tissue repairing or wound healing. Moreover, our approach can be extrapolated to almost any polymer and biopolymer ordered pore array fabrication.

61.41 +e, 87.85J, 81.05Rm, 82.45Cc, 81.16Rf, 81.10Fq, 81.10Dn

1. Introduction

Well defined nanopore arrays are of high interest to be used as templates for the preparation of functional nanowires with, for example, thermoelectric[1-3] or magnetic properties[4]; or as an effective material for direct applications (for instance in biomedicine [5-7]). In this last sense, they are particularly attractive as scaffolds for different types of cells, which frequently evidence important advantages against their planar counterparts [6, 8, 9]. It is well known that cell adhesion, proliferation, and migration are influenced by the nanoscale topography since cells are able to recognize nanoscopic features, especially those in the range of hundreds of nanometers [10, 11]. Moreover, being able to control the diameter of the pores, their distance and their depth is of high importance since proliferation of cells strongly depends on nanopore dimensions, as has been demonstrated in Porous Anodic Aluminum Oxide (AAO) templates [12]. AAO templates usually possesses pore diameters ranging from 20 to 400 nm [13-15], lattice constants varying in the 50 to 500 nm range, and pore depths from few hundreds of nm up to several hundreds of μm. This variability, the fact that these templates are obtained by self-assembly and, moreover, that the surface obtained can cover large areas (even m^2), makes porous alumina a template that has been deeply study for all these applications. However, AAO are rigid and fragile, and therefore, their use as scaffold for tissue repairing or wound healing is limited. Thus, from the practical point of view, it is of high interest to develop nanostructured surfaces with the attractive morphological characteristics of the AAO templates, but presenting properties like biodegradability, easy functionalization, capability for drug, micelle or nanoparticle delivery, mechanical flexibility, and so on. Polymers like poly(vinyl alcohol) (PVA) fulfill that.

Two-dimensionally ordered nanoporous surfaces composed of “commodity” polymers can be prepared by block-copolymer self-assembly [16], by colloidal crystal-assisted capillary nanofabrication [17], by templating metal pillar arrays [18], by plasma etching using masks [19], by nanoimprint lithography [20], by beam-lithographic techniques [21], etc. However, by means of some of those approaches (such as beam lithographies or block copolymers) it is difficult to nanostructure many biocompatible polymers. Other approaches, such as colloidal crystal-assisted capillary nanofabrication, do not allow varying the pore aspect-ratio. Therefore, template-based techniques, seems to be the most promising approaches for nanostructuring biocompatible polymers. Among templates, AAO is standing out due to the large patterned areas and tailored interpore distances

and pore aspect-ratios. However, the AAO fabrication is usually time and resource consuming and current template-based nanofabrication approaches imply the destruction of the AAO template, reducing their possibilities for re-use, and hindering a potential industrial up-scaling of the process. In this sense, it is generally accepted that it is crucial to develop cost-effective nanostructure fabrication methods capable of being up-scaled to an industrial level. Interesting procedures have been reported for the non-destructive fabrication of high-aspect ratio nanopillar arrays [22, 23]. However, no attempt have been made (to the authors knowledge) for developing a high output method for macro-sized polymer nanopore arrays exceeding the aspect-ratios achievable with nanoimprint lithography molds.

Thus, we propose here a simple, fast, easy and high-throughput fabrication method for obtaining nanoporous polymeric surfaces by replicating the tunable porous alumina, see **Fig. 1.** Our method is based on three-stages **(Fig. 1)**: First, preparing a hard template **(Fig. 1a),** in our case, porous alumina AAO with the desired pore diameter. Second, a polymer is infiltrated inside the alumina nanopores **(Fig. 1b)** to prepare its negative replica. And third, after releasing the prepared polymer nanopillar array **(Fig. 1c)**, it is used as a negative master for achieving a polymeric replica of the initial porous alumina structure **(Fig. 1d)**. This ordered nanoporous polymer **(Fig. 1e)** should be detached from the nanopillar surface with the use of tweezers so it could be reused many times, which would enable the high-throughput production of ordered polymer nanopore arrays.

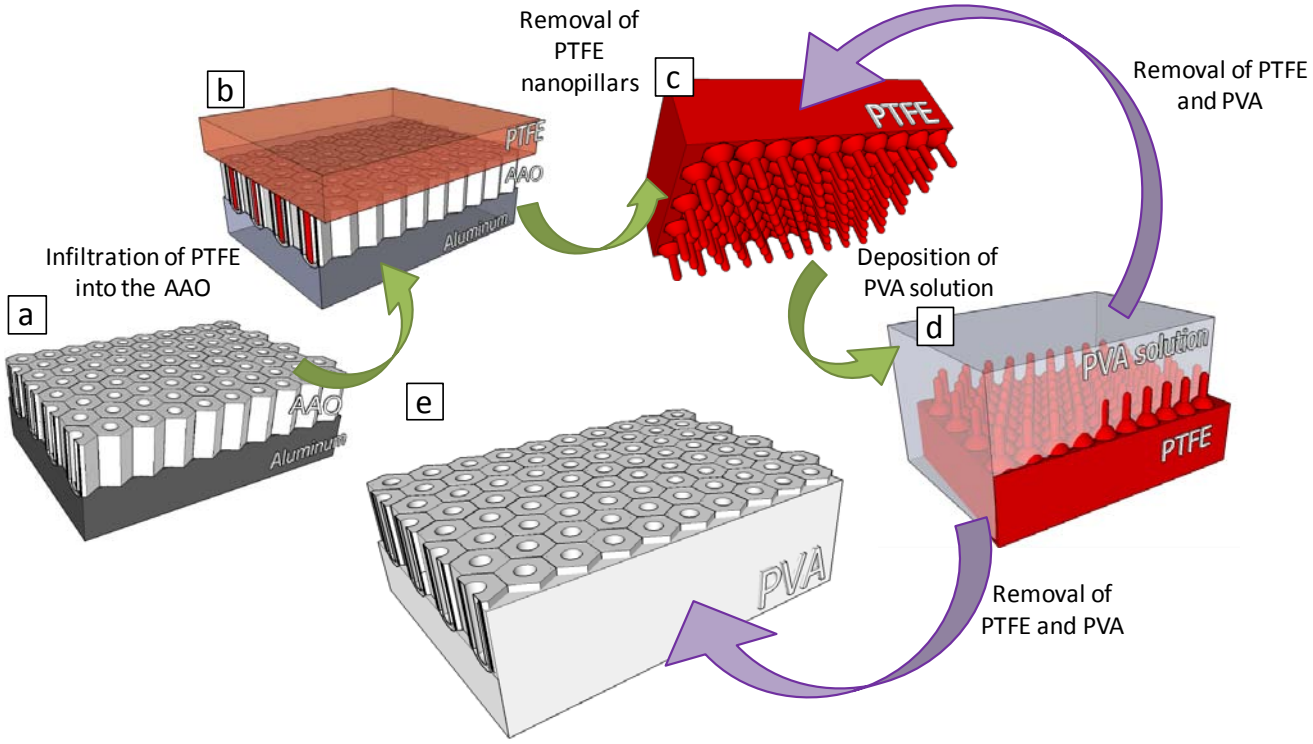

Figure 1. Schematic diagram of the replication process of nanopores alumina surface to obtain a nanopores array made of the biocompatible polymer PVA. First, a nanoporous hard template of Anodic Aluminum Oxide (AAO) is synthesized (a); then a polymer melt is infiltrated into the nanopores (b) and after removal of the template, a polymer nanopillar array is obtained (c). The nanopillar array is used as a negative mold for replicated fabrication of the original hard template. In this step, a polymer solution is deposited on the nanopillar array (d) and once the solution is dried, the second polymer is detached from the nanopillar array giving rise to an ordered nanopores surface (e) and to the pristine nanopillar array (f) which can be reused for another porous array fabrication.

In order to perform the process mentioned above different challenge must be solved: a) infiltration of a polymer with low adhesion and friction properties, good wettability, insoluble in the solvents used in the following steps, and with enough mechanical resistance that can be re-used as a master for several runs; b) nanostructure a functional polymer with interesting conditions as biomaterial, and c) finally, release the nanostructured polymer without affecting the inverse mold. For that, it is essential to reduce the interaction between nanopillars and polymer pore walls. Hence, a material with low friction and adhesion properties is needed for the mechanical removal. Thus, poly(tetrafluorethylene) (PTFE) sounds ideal for constituting the inverse nanostructured mold (the nanopillared surface [24]. Moreover, the PTFE present certain advantages against other typically used hydrophobic polymers, such as PDMS: *(i)* PDMS is a cross-linked elastomer, so it is highly flexible at room

temperature. And such flexibility could cause problems regarding the achievable aspect ratios (the nanopillar aggregation depends on the flexibility of the polymer the pillar is composed of), and also at the demoulding stage at which the PDMS nanopillars could be broken easier than the PTFE nanopillars due to the higher mechanical rigidity of the latter. *(ii)* On the other hand, PDMS elastomers are, as mentioned, usually crosslinked polymeric networks. This means that for preparing the PDMS nanopillar array one should infiltrate the linear PDMS polymer into the AAO nanopores and then perform the cross-linking chemical reaction by means of a curing agent. These curing agents are therefore multifunctional molecules that react with more than one polymer chain. Thus, a chemical reaction is established and as most of these chemical reactions will not be fully efficient, so a non-reacted fraction of curing agent will remain in the PDMS network. Taking into account that our final material should have biomedical applications, this contamination issue is a problem. Furthermore, PTFE is bio-inert [25], hydrophobic [26], shows a high degradation temperature under different atmospheres [27-29], and it is completely insoluble in all solvents. However, its high melt-viscosity even at high temperatures (10^{11} P at 380 ºC) makes common macroscopic molding methods impossible for PTFE. Thus, the nanostructuration of PTFE is not trivial either due to its insoluble nature and its inability to macroscopically flow; that is why only a handful of papers have been reported on the preparation of ordered nanostructures made up of PTFE [30-32]. In this sense, we show that the procedure used here is highly efficient for preparing ordered PTFE nanostructures from melts.

Besides the difficulty for PTFE nanostructuration, it must be also taken into account the fact that the PTFE surfaces are in general non-wettable, which should hinder the possibilities of PTFE as template. A poor wetting of the second polymer onto the PTFE nanostructure implies an incomplete replication of its morphology. It is well known that generally, the wettability of a solid surface is controlled by both its surface energy [33] (in terms of the surface chemical composition) and its geometrical architecture [34]. PTFE is known to be one of the materials with the lowest surface energy. In consequence, common liquids usually present a higher surface energy than that of the PTFE surface and thus do not wet it properly. Moreover, when a nanoscopic roughness is induced on an originally hydrophobic surface, its wettability decreases even more, according both to Wenzel [35] and Cassie-Baxter [36] models. The problem is magnified when one considers the fact that many of the biocompatible polymers must be nanomoulded from high-surface-energy aqueous solutions. In this work, the problem of the

PTFE wetting is also solved thanks to a surface chemical modification of the PTFE nanopillars that is induced during their nanostructuration within the AAO, as revealed by confocal Raman spectroscopy and attenuated total reflectance Fourier transform infrared spectroscopy (ATR-FTIR).

Thus, for demonstrating the efficiency of the method, we use the functionalized PTFE nanopillar arrays as masters for the fabrication of ordered large-area nanopores surfaces composed of added-value polymers, such a biocompatible polymers (PVA, in this case). Both the patternable area and the structural dimensions of the pore array are directly given by those of the original hard template, so, areas of cm^2 and sub-100 nm periods and 25-400 nm pore diameter range could be obtained.

2. Materials and Methods

Ordered AAO templates were prepared by a two-step electrochemical anodization of aluminum [13, 37]. Firstly, ultrapure (99.999%) aluminum foils (Advent Research Materials, England), were cleaned and degreased by sonication in acetone, water, isopropanol, and ethanol. Foils were then electropolished in a solution of perchloric acid/ethanol (1/3) under a constant voltage of 20 V, and after that, the first anodization was carried out. An aqueous solution of phosphoric acid (1 wt. %) was used as electrolyte, under a constant potential of 205 V. The temperature was carried out at 4.5 ºC for 6 h. Aluminum oxalate was also added to the solution (0.01 M) for stabilizing the reaction as reported elsewhere [37]. Then, the first anodic layer was removed by chemical etching in a mixture of phosphoric acid (7 wt. %) and chromic oxide (1.8 wt. %). Finally, the second anodization was performed for 2 minutes in the same conditions as the first one.

For the PTFE infiltration, the AAO template was cleaned by sonication in solvents with different polarity (water, ethanol, and acetone). Then, the adsorbed organic molecules were removed from the pore walls by heating the AAO template in vacuum. These molecules decrease the surface energy of the substrate, hindering the infiltration of the polymer. Once that the template was completely cleaned, a piece of commercial PTFE (PTFE, DuPont) was placed onto the surface of the AAO template at a certain temperature, so the infiltration of the molten PTFE takes place [38-41]. Experimentally, the infiltration was carried out following these steps (see, Supporting information, Fig. S1): In the first stage, the AAO template is heated in a vacuum oven (Brother XD-

1200) at the constant heating range of 4 ºC/min until 400 ºC. As mentioned, at high temperature organic molecules are removed from the alumina pore walls. In the second step at 400 ºC, a solid piece of PTFE was placed onto the AAO and when the PTFE was apparently molten, a slight pressure was applied. Then, the system was kept at 400 ºC for 40 minutes. Finally, the sample was cooled at 3 ºC/min down to 350 ºC and then at 1 ºC/min down to 250 ºC.

Once the PTFE is crystallized within the nanopores, the polymeric nanopillar array was removed from the AAO template. For that, the aluminum substrate was dissolved in an acidic solution of $CuCl_2$, and the AAO was dissolved in NaOH 10 wt. %.

All the prepared samples were morphologically characterized by scanning electron microscopy (SEM) (Hitachi S-800). The water contact angles were measured with the drop shape analysis system Easy Drop Standard from Krüss. The Raman study was carried out with the use of a confocal micro-Raman (Witec alpha-300R). Raman spectra were obtained using a micro-Raman system with a 532 nm excitation laser and a 100x objective lens (NA=0.9). The incident laser power was 0.5 mW. The optical resolution diffraction of the Confocal Microscope was limited to 200 nm laterally and 500 nm vertically. Raman spectral resolution of the system was down to 0.02 wavenumbers. The microscopy stage was mounted in a piezo-driven scan platform having 4 nm lateral and 0.5 nm vertical positioning accuracy. The piezoelectric scanning table allows 3D steps of 3 nanometers, giving a very high spatial resolution for the confocal Raman microscopy. The microscope base was also equipped with active vibration isolation system, active 0.7 – 1000 Hz. Collected spectra were analyzed by using Witec Control plus Software. Attenuated total reflectance Fourier transform infrared spectra were recorded at ambient temperature on a Spectrum One FTIR spectrometer of Perkin Elmer equipped with an internal reflection element of diamond using an accumulation of 4 runs and the same pressure of the crystal on the surface in each sample.

For the preparation of the ordered arrays of PVA nanopores, an aqueous 10 wt. % solution of PVA (M_w = 94 000 g/mol, 99 % hydrolyzed, supplied by Aldrich, Ltd.) was placed onto the surface of the PTFE nanopillar arrays. The water was evaporated in vacuum overnight and finally, the PVA films were mechanically removed from the PTFE by ripping them off with tweezers

3. Results and Discussion

The obtained AAO templates were a polydomain hexagonal array of cylindrical nanopores, where the pores were 120 nm in diameter, around 300 nm in length, and the interpore distance was 430 nm, as can be observed in Fig.2. These characteristic dimensions (pore diameter, interpore distance and pore length) were selected for achieving a PVA nanohole array of the same dimensions. Polymeric nanostructures with nanoscopic features having sizes in this range are known to be well recognizable by living cells [10].

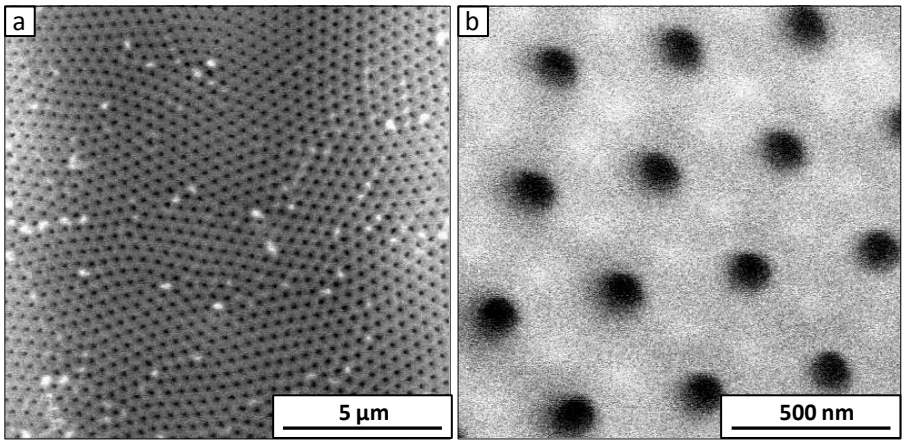

Figure 2. SEM micrographs of the surface of 120 nm porous AAO template: (a) large view where polydomain structure can be seen. (b) Hexagonal pore arrangement within an ordered region.

The method used for infiltrating PTFE into the AAO nanopores is based on the wetting behavior of liquid PTFE over the AAO pore walls. Briefly speaking, the PTFE melt is a low surface energy liquid that spontaneously tends to wet the pore walls of the high surface energy AAO template [38, 39]. Although the high molecular weight of the commercial PTFE (10^6-10^7 g/mol) makes the polymer non-flowable, if the PTFE piece is pressed against the template surface at the beginning of the infiltration process, polymer chains come in contact

with the pore walls and spread through it [31]. Once the infiltration takes place, the PTFE is crystallized at low cooling rate (1ºC/min) in order to improve its crystalline characteristics. It is well known that a higher degree of crystallization, more perfect, and larger crystals are obtained when the dynamical crystallization is performed at low cooling rates. And as those characteristics are improved, a more resistant material is obtained.

Fig. 3 shows the obtained PTFE nanopillar array. The nanostructured area extends over cm^2, as can be appreciated in Fig. 3a. The SEM micrographs of the nanostructure (Fig. 3b-d) demonstrate a polymeric surface having a negative replica of the AAO pattern. The PTFE pillar array shows an hexagonal closed-packed symmetry over 10 to 20 inter-pillar distances (Fig. 3c and 3d), while on a larger scale, a typical polydomain structure of the AAO can be clearly observed (Fig. 3b). The nanopillars are 120 nm in diameter and approximately 350 nm in length (Fig. 3d), which is the maximum length for having free standing PTFE nanopillars. Higher aspect ratio nanopillars tend to bend and aggregate, losing the ordered character of the nanostructure (see supporting information Fig. S2), in such a way that become unsuitable for nanomolding the persuaded ordered array of polymer nanopores. On the other hand, the inter-pillar distance is 430 nm, and the density of nanopillars is around 10^9 pillar/cm^2. To the best of our knowledge this is the first time that free-standing hexagonal arrays of semicrystalline PTFE nanopillars is reported. Examples of nanostructuration of soluble PTFE can be found in the literature [42], however, it should be emphasized that the soluble PTFE is an amorphous polymer, and thus leads to materials with significantly lower mechanical, chemical and thermal properties. Regarding the nanofabrication method, it is worth noting that the PTFE nanopillar array has been prepared by means of an easy, efficient, safe and environmentally compatible procedure.

The semicrystalline nature of the PTFE nanopillars can be ensured looking to their thermal resistance. It is well known that the glass transition temperature (T_g) is around 250 °C. In fact, that is the reason why the material commonly known as “soluble Teflon” can be operated only until that temperature. Soluble Teflon is an amorphous PTFE-based copolymer, so the maximum temperature applicable before losing the morphology and structural dimensions of the material is precisely the T_g, that is, around 250 °C. In contrast, for this work, the

homopolymer PTFE was used. In order to evaluate the thermal stability of our nanostructured material, we perform a thermal resistance experiment to it. Specifically, the nanopillar array was annealed at 300 °C for 60 min, and then, its morphology was analyzed by SEM. The nanopillars maintained their morphological integrity without apparent damage in the nanostructure (supporting information S4), which means that the PTFE must be semicrystalline to support 300 ºC.

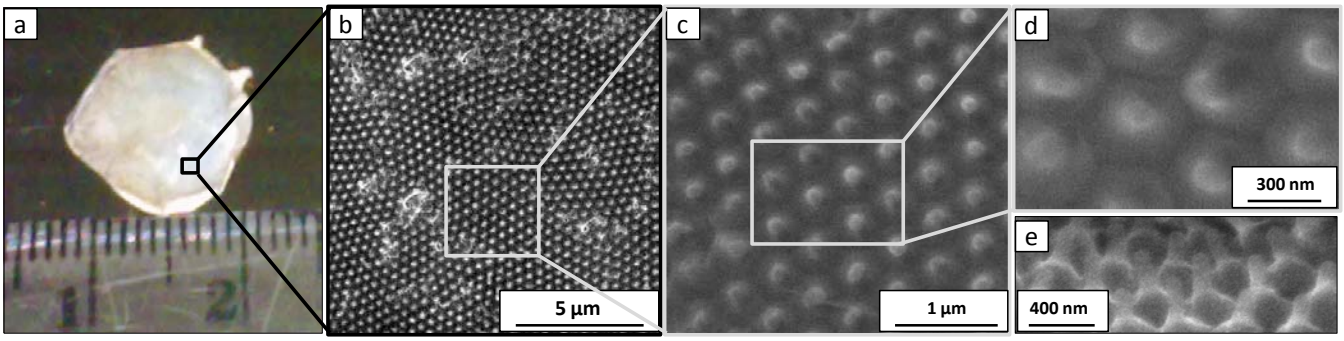

Figure 3. (a) Photograph of the PTFE nanopillar array where its macroscopic extensions can be appreciated. SEM micrographs of the surface (b, c, and d) and lateral (e) side view of the prepared PTFE nanopillar array, they resemble to the surface of a gecko feet.

In order to check the wettability of the nanostructured PTFE, surface contact angle (θ) measurements were carried out. The contact angles for distillated water over bulk and over a nanostructured PTFE surface are of θ_{bulk} = 95 ± 7° ; $\theta_{nanoPTFE}$ = 91 ± 6° for droplet volumes of V_{bulk} = 6.93 ± 0.04 µl; $V_{nanoPTFE}$= 6.42 ± 0.04 µl, see Fig. 4. These values highlight that upon nanostructuration of the surface the PTFE surface becomes slightly more hydrophilic.

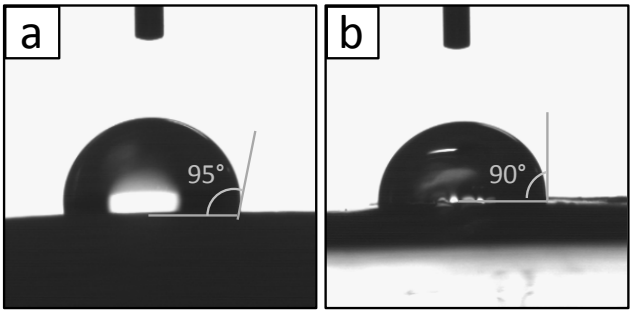

Figure 4. Optical microscope images of water droplets on PTFE samples: (a) bulk PTFE and (b) nanostructured PTFE.

Our results seem to be in contrast with the Wenzel and Cassie-Baxter models which are the two main models that describe the wetting of textured surfaces. These models predict that the contact angle increases with the surface roughness for originally hydrophobic materials (independently on fractional areas of solid-liquid and liquid-vapor interfaces, in the case of the Cassie-Baxter model). This fact has been experimentally observed [42-45]. It means that the presence of the nanostructures on the PTFE surface should decrease its wettability, and thus, the contact angle of the nanostructure should be higher than that of the unstructured PTFE surface. However, in our materials θ_{bulk} is similar or higher than $\theta_{nanoPTFE}$. In this sense, we calculated the contact angle value of the PTFE nanopillar array according to Wenzel model (θ_{Wen}) using the θ of the un-modified planar PTFE surface (θ_{bulk}) and geometrical aspects of the nanostructure. According to that model, the θ of the PTFE surface would increase from 95° to 99° due to the presence of the nanopillars. However, we found just the opposite situation: the experimental θ of the nanopillar array was of 91°. This fact could mean that in our case, that the nanostructuration is playing a minor role when compared to the other factor affecting the wettability of a solid surface, i.e. the surface energy [33]. As it is known, the surface energy is related to the chemical nature of the materials, so the observed contact angle reduction could be ascribed to a surface chemical modification of the material. In order to confirm this hypothesis, a high resolution depth profiling confocal Raman analysis and ATR-FTIR spectroscopy experiments were performed on the nanostructured PTFE surface.

Fig. 5a and Fig. 5b show the depth-profiling Raman spectra of bulk PTFE and nanostructured PTFE, respectively. Within the acquired multi-spectrum depth profiling file for the nanostructured PTFE, two different types of spectra can be distinguished depending on the analyzed depth: the spectra collected at the deepest region correspond to that of bulk PTFE; while the spectra collected at the surface (that is, at the nanopillar region) correspond to a modified PTFE (Fig. 6c). In the comparison of a spectrum from the bulk part against the surface, two main differences can be remarked: first the appearance of higher fluorescence and lower signal/noise ratio at the surface related to both the nanostructure of the surface and the dispersion of the laser signal due to the surface topography; and second, the appearance of new Raman modes in the nanopillars in addition of the PTFE ones. Among the new modes located at the nanopillars, the more characteristic ones appear around 2900 cm^{-1} and correspond to the stretching vibrations of the C-H bond. The C=C stretching can be also distinguished around 1700 cm^{-1}.

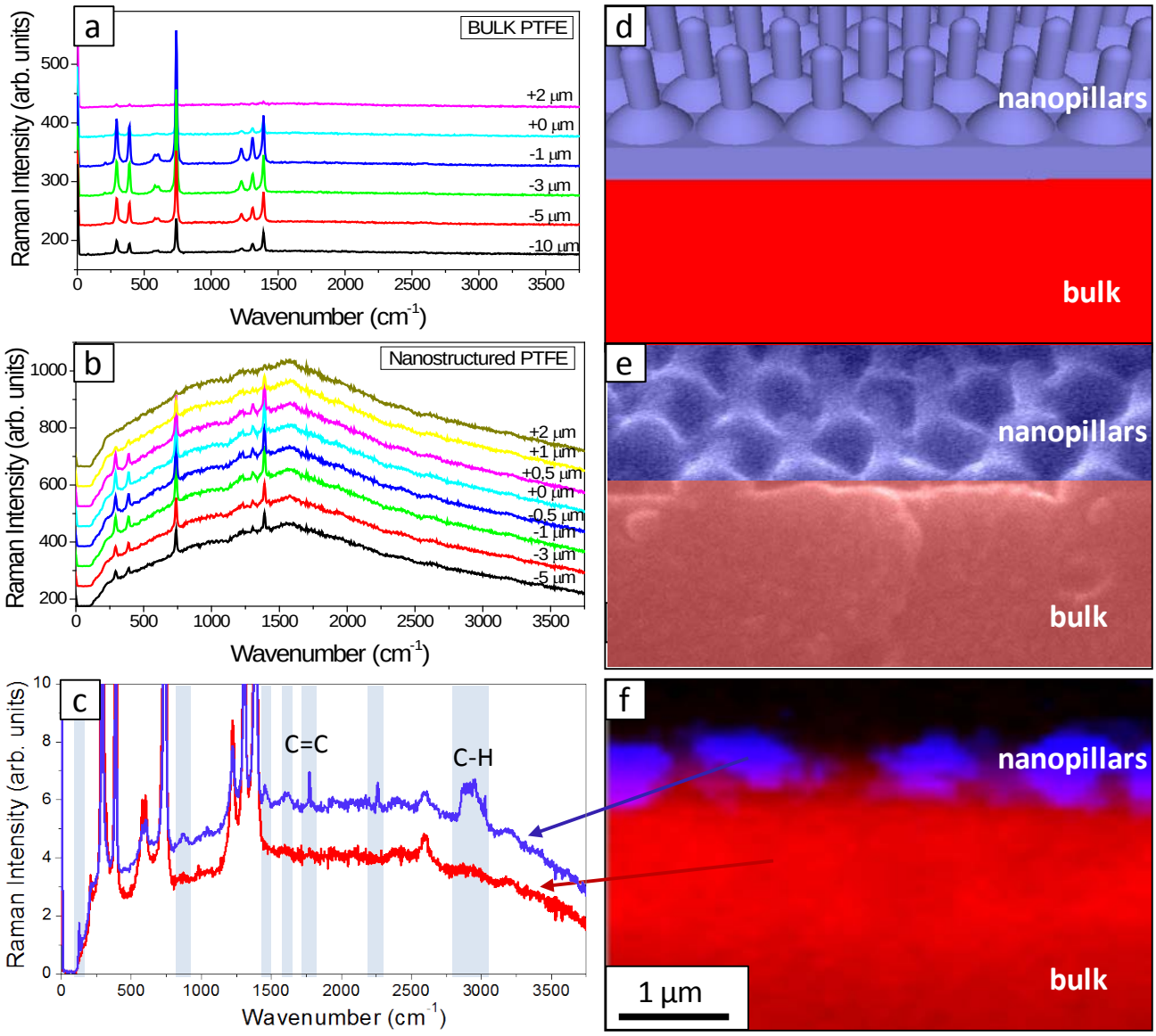

Figure 5. Raman spectra along the z-axis for bulk PTFE (a) and PTFE nanostructure (b), (c) Comparison of averaged Raman spectra of surface and inner part. The grey regions highlight the differences between them. Schematic representation (d), sketch of the cross section of the nanostructured surface (e) and SEM image of the cross-section of the real surface (f) Raman image of the sample depth profiling, the blue zones corresponds to where the blue spectra is obtained, while the red corresponds to the zone where the red spectra are obtained..

PTFE is a remarkably inert material, however, it can be chemically modified by means of various procedures, such as wet chemical reactions, electrochemical reductions, plasma treatment, ion or electron beam treatments, laser ablation, and so on. Our nanostructured PTFE surface was formed in touch with the AAO pore walls during the infiltration process at 400 °C, and during this process PTFE could interact with the any of the reactive species present in the AAO templates, i.e. hydroxyl groups and the oxygen of the pore wall, the occluded water, the PO^{4-} anions [46], or even with the own alumina. It is difficult to determine exactly the chemical reactions taking place at such interface at 400 ºC, but what seems clear is that one or some of them lead to the defluorination of PTFE and to the formation of C-H and C=C bonds. A plausible explanation for this behavior is the conversion of Al_2O_3 to AlF_3 by the exposure to a fluorinated surface. AlF_3 has much lower Gibbs free energy of formation than Al_2O_3 [47].Since AlF_3 is far more stable than Al_2O_3, the alumina surface will trap the F^- from the polymer producing its defluorination and forming a layer of AlF_3 at the interface alumina/polymer. These kind of defluorination and formation of both saturated and unsaturated carbonaceous groups in PTFE surfaces has been observed when treated with strong chemical reducing agents, such as sodium/naphthalene complex [48], lithium-liquid ammonium system [49], or benzoin dianions [50]. All this reactions are known to darken the originally white PTFE. [50] And, they will explain the brownish color that our template has after nanostructuration, see Fig. 3a. In our case, the defluorination of the PTFE takes place exclusively at the PTFE-AAO interface, as deduced from the Raman depth-profiling, since the bands at 2900 cm^{-1} and 1700 cm^{-1} can be only appreciated at the region closed to the surface, this is, in the nanopillared region. The rest of the sample presents the Raman signal of bulk PTFE.

In order to demonstrate that the used solution for the alumina removal (NaOH 10 wt.%) was not responsible of the observed chemical modifications of the PTFE nanopillars, we subjected a planar PTFE surface to that solution, and we analyzed the surface composition by confocal Raman Scattering. We observed that such treatment did not induce the appearance of the new Raman bands observed in the sample with nanopillars at around 1700 cm^{-1} and 3000 cm^{-1}) (see supporting information).

The surface chemical modification of our PTFE nanopillars is additionally confirmed by ATR-FTIR spectroscopy (Fig. 7). Fig. 7a shows the complete ATR-FTIR spectra collected for nanostructured and bulk

PTFE. Both show the characteristic peaks at 1145 and 1201 cm^{-1}, which correspond to the C-F_2 asymmetrical and symmetrical stretching [51]. It is worth noting that the intensity of these peaks weakened after the nanostructuration process (Fig. 7c), which can be associated to defluorination of the PTFE surface. Furthermore, it can be also observed the stretching of C-H (at 2849 and 2919 cm^{-1}), C=C (at 1646 cm^{-1}), and O-H (at 3394 cm^{-1}) bonds (Fig. 7a), which corroborate such defluorination.

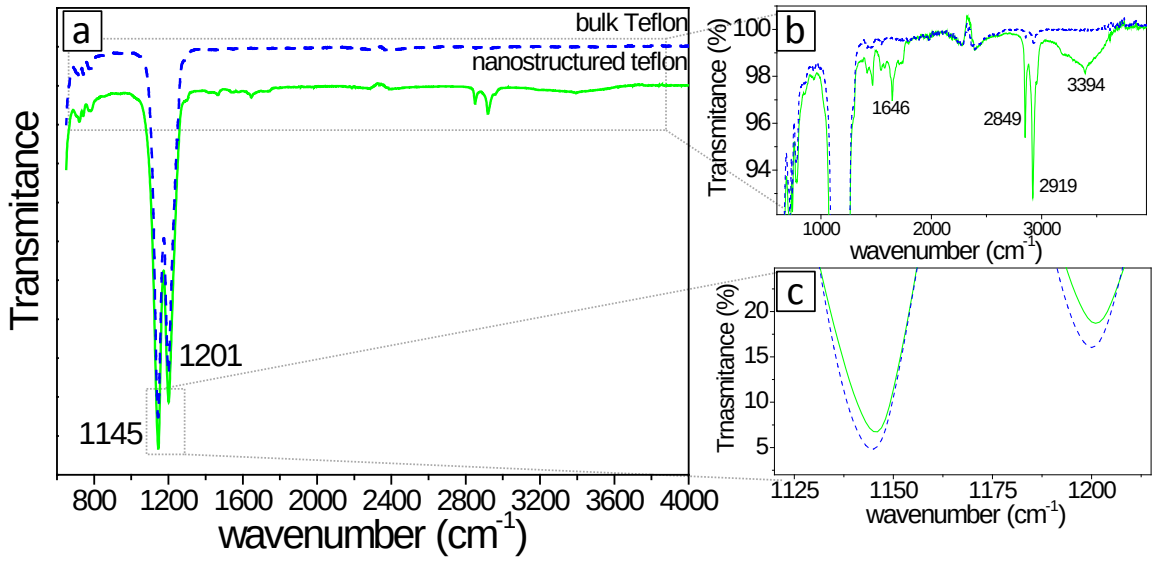

Fig. 7. ATR-FTIR spectra of bulk (dashed blue line) and nanostructured (continuous line) PTFE: (a) whole collected spectra. (b) Detailed view of the C-H (at 2849 and 2919 cm^{-1}), C=C (at 1646 cm^{-1}), and O-H (at 3394 cm^{-1}) stretching bands present in the spectra of nanostructured PTFE surface. (c) Detailed view of the intensity of the C-F stretching bands for bulk (dashed blue line) and nanostructured (continuous line) PTFE.

The first consequence of the observed defluorination is the increase of the PTFE surface energy, which leads to the lower contact angles measured for water onto the nanostructured surface. Thus, the more wettable PTFE surface can be used as template for the fabrication of a new nanopore arrays composed of a second polymer, even of a hydrophilic one. In order to show this particular point, the fabrication of ordered arrays of PVA nanopores mimicking the porous alumina surface structure has been carried out.

Fig. 8a shows a photograph of the nanostructured PTFE surface and its PVA negative pattern. The PTFE pattern has been completely transferred to the PVA, in such a way that an array of nanopores has been formed, as can be observed in Fig. 8b and 8c, where low and high magnification SEM micrographs of the obtained PVA nanopore array are shown. The inset in Fig. 8c shows Fourier transform of the images, from which the hexagonal symmetry of the pore arrangement can be deduced. PTFE nanopillar array is an efficient nanomold since allows obtaining biocompatible polymer replicas of the original AAO. The dimensions of the new nanostructure are: pore diameter: 140 nm; and interpore distance: 430 nm. Note that features of such characteristic dimensions are known to be well recognizable by human cells [10].It is important to notice that the PTFE nanopillar array is unaltered after detaching the PVA as can be appreciated in Fig. 7d. Its surface is completely clean and does not present apparent morphological damages. Thus, the nanostructure could be reused for templating more PVA nanopore arrays. Fig. 8e shows the PVA pore array obtained in a second nanomolding. As observed, the pattern is again completely transferred to the PVA surface.

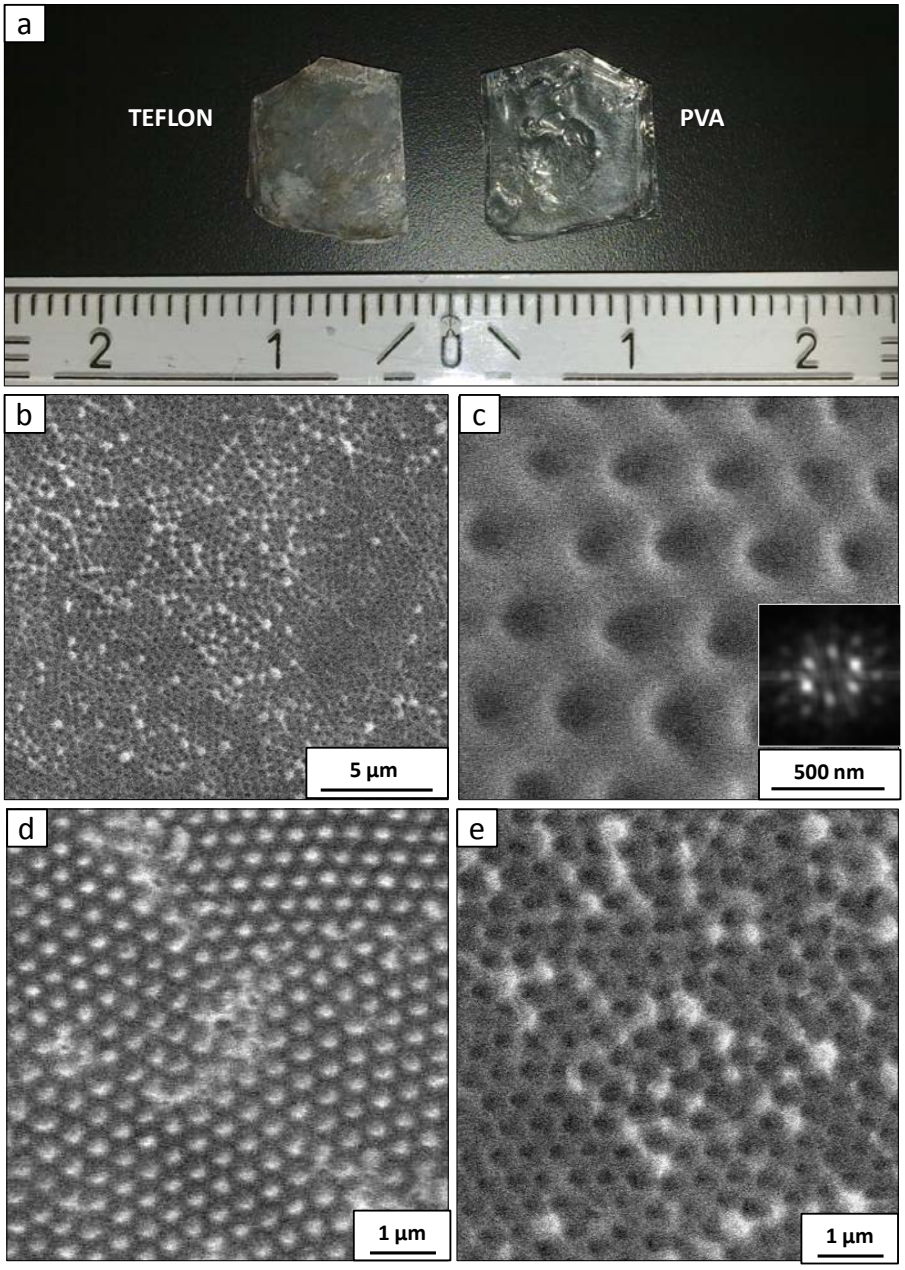

Figure 8. (a) Photograph of the nanostructured PTFE surface (left) and its negative PVA pattern. Large view (b) and detailed view (c) of the prepared hexagonal array of PVA nanopore array obtained by SEM at different magnifications. The inset in (c) correspond to the Fourier transform of the image. (c) SEM image of the unaltered surface of PTFE nanostructure after detaching the PVA nanopores array. The PTFE nanostructure is reused for the preparation a second PVA nanopore array, which is shown in (e).

It is important to highlight that the fabrication process for PVA nanopore array is notably economic and allows obtaining big areas (Fig 8a). The whole fabrication procedure reported in this work allows developing the high-throughput fabrication process of biocompatible nanostructures that can easily integrate some kind of dressing for tissue repairing or drug delivery agent. Moreover different patterns could be integrated in a sample by using adequate templates having designed pores size and interpore distance.

4. Conclusions

In summary, we have developed an efficient methodology for the simple fabrication of ordered nanoporous surfaces composed of biocompatible polymers (PVA, in this case) which allows their high-throughput production. The procedure is based on a two-stage replication of templates. For that we prepared free-standing hexagonal arrays of semicrystalline PTFE (PTFE) nanopillars which were subsequently used for templating the PVA nanopore arrays. This PTFE nanostructuration process induces changes in the chemical composition of the nanopillars: a fraction of the fluorine atoms are eliminated and new C-H, C=C, and O-H bonds are formed as reveled by depth profiling confocal Raman spectroscopy and ATR-FTIR. The direct consequence of this modification is that the nanostructured surface becomes more slightly hydrophilic. This increase in the hydrophylicity could in part the responsible of the good pattern transfer from the hydrophobic PTFE to the hydrophilic PVA.

The morphology of the prepared PVA nanopores surface is almost a replica of that of the original AAO hard template. Thus, the nanopores are 130-140 nm in diameter and interpore distance is 430 nm. The fabrication process for PVA nanopore array is notably economic and allows obtaining areas of cm^2. Furthermore, due to the fact that the template is not destroyed in the PVA nanomoulding, it can be reused for preparing additional nanopore arrays. It should be emphasized that our approach can be extrapolated to other polymer and biopolymer pore array fabrication simply substituting of the PVA solution for the solution or the precursor monomer of the taget polymer. The developed procedure can be up-scaled to the industrical level for a high-throughput production of two-dimensional scaffolds for tissue repairing, wound healing, or drug delivery.

Acknowledgments

Authors want to thank the ERC 2008 Starting Grant number 240497 and project MAT2010-21088-C03-01 for financial support. Dr. Helmut Reinecke is acknowledged for his help with the FT-IR ATR measurements.

Supplementary data

Ordered arrays of polymeric nanopores by using inverse nanostructured PTFE surfaces

Jaime Martín[1], Marisol Martín-González[1,*], Adolfo del Campo[2], Julián J. Reinosa[2], and José Francisco Fernández[2]

[1] Instituto de Microelectrónica de Madrid (CNM-CSIC), Isaac Newton 8, PTM, E-28760 Tres Cantos, Madrid, Spain
[2] Instituto de Cerámica y Vidrio (ICV-CSIC), Kelsen 5, 28049 Cantoblanco, Madrid, Spain

E-mail: marisol@imm.cnm.csic.es

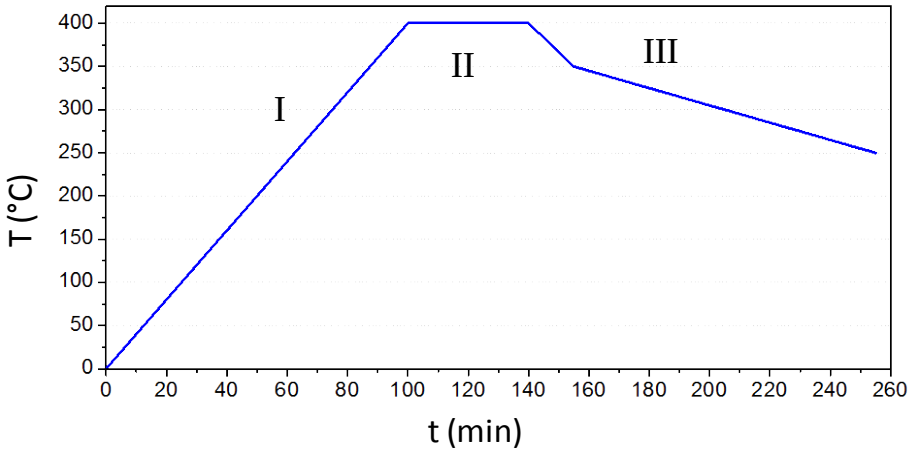

Figure S1. Applied temperature program for the infiltration of molten PTFE into the nanopores. (I) The AAO is heated up to the infiltration temperature. (II) The infiltration takes place at a constant temperature. (III) Crystallization of the PTFE nanostructure.

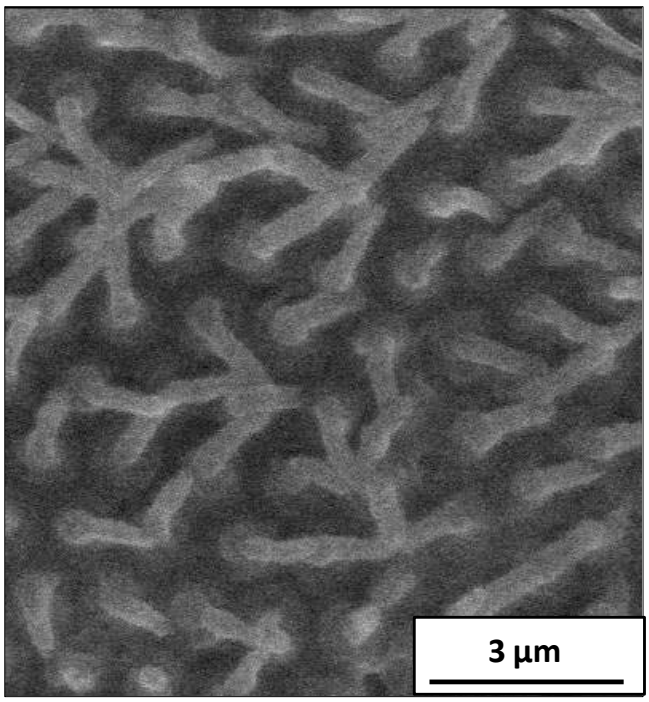

Figure S2. SEM image of a PTFE nanostructured surface where the nanopillars are aggregated as a consequence of their high aspect-ratio (around 5).

In order to demonstrate that the used solution for the alumina removal (NaOH 10 wt. %) was not responsible of the observed chemical modifications of the PTFE nanopillars, we subjected a planar PTFE surface to that solution for 2 h, and we analyzed the surface composition by confocal Raman Scattering. We observed that such treatment did not induce the appearance of the new Raman bands observed in the sample with nanopillars at around 1700 cm^{-1} and 3000 cm^{-1}) (see supporting information)".

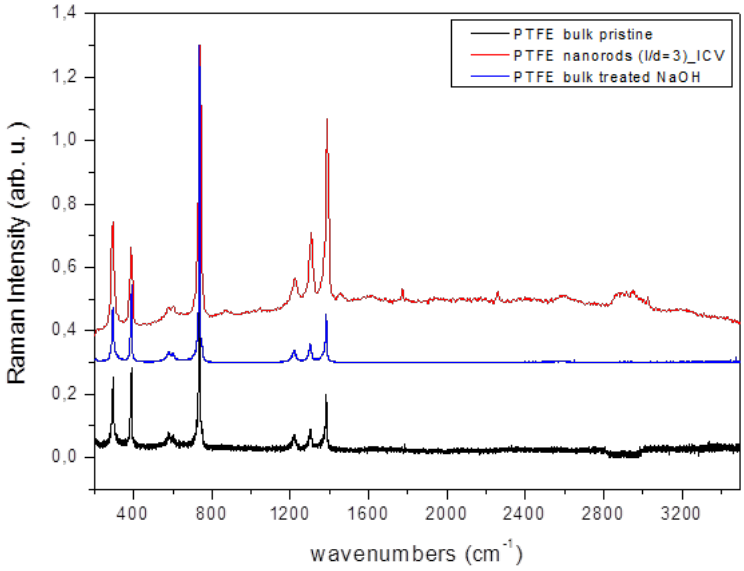

Fig S3. Raman spectra of pristine bulk PTFE (black line), bulk PTFE subjected to NaOH 10 wt.% for 2 h (blue line), and the averaged spectra of surface part of the sample with nanopillars (red line).

We can assert that the PTFE nanopillars are semicrystalline looking just to their thermal resistance.It is well known that the glass transition temperature (Tg) is around 250 °C. In fact, that is the reason why the material commonly known as “soluble Teflon” can be operated only until that temperature. Soluble Teflon is an amorphous PTFE-based copolymer, so the maximum temperature applicable before losing the morphology and structural dimensions of the material is precisely the Tg, that is, around 250 °C. In contrast, our PTFE was the homopolymer PTFE. In this sense, we perform a thermal resistance experiment to our PTFE pattern, which afterwards was not included in the manuscript. In concrete, the nanopillar array was annealed at 300 °C for 60 min, and then, its morphology was analyzed by SEM. As can be observed in the following SEM micrographs, the nanopillars maintain their morphological integrity without apparent damage in the nanostructure, which means that the PTFE must be semicrystalline to support 300 ºC.

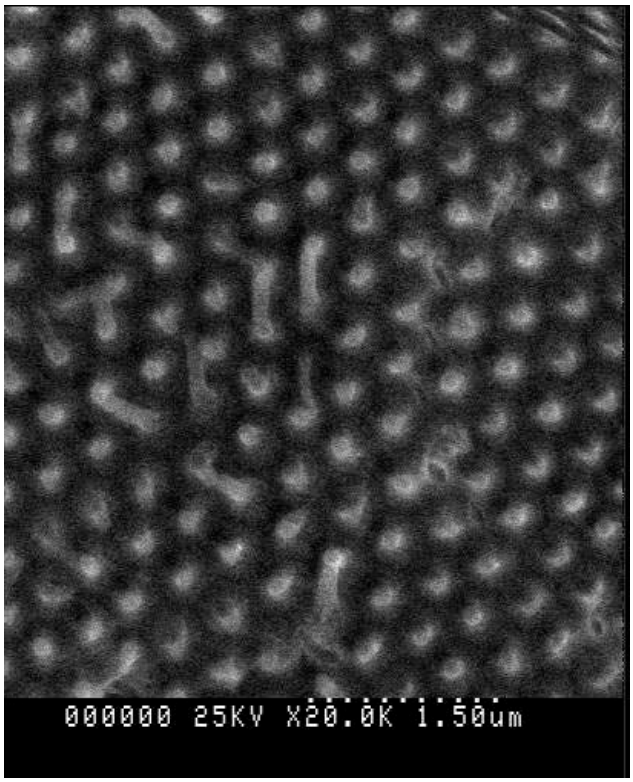

Fig S4. SEM image of PTFE nanopillar array annealed at 300 °C for 60

References

[1] Martín-González M, Prieto AL, Gronsky R, Sands T and Stacy AM. 2003 *Advanced Materials* **15** 1003-6.
[2] Martín-González M, Prieto AL, Knox MS, Gronsky R, Sands T and Stacy AM. 2003 *Chemistry of Materials* **15** 1676-81.
[3] Martín-González M, Snyder GJ, Prieto AL, Gronsky R, Sands T and Stacy AM. 2003 *Nano Letters* **3** 973-7.
[4] Martín J, Vázquez M, Hernández-Vélez M and Mijangos C. 2008 *Nanotechnology* **19** 175304.
[5] La Flamme KE, Popat KC, Leoni L, Markiewicz E, La Tempa TJ, Roman BB, Grimes CA and Desai TA. 2007 *Biomaterials* **28** 2638-45.
[6] Peng L, Eltgroth ML, LaTempa TJ, Grimes CA and Desai TA. 2009 *Biomaterials* **30** 1268-72.
[7] Aw MS, Simovic S, Addai-Mensah J and Losic D. 2011 *Journal of Materials Chemistry* **21** 7082-9.
[8] Ferraz N, Nilsson B, Hong J and Karlsson Ott M. 2008 *Journal of Biomedical Materials Research Part A* **87A** 575-81.
[9] Popat KC, Leoni L, Grimes CA and Desai TA. 2007 *Biomaterials* **28** 3188-97.
[10] Grimm S, Martin J, Rodriguez G, Fernandez-Gutierrez M, Mathwig K, Wehrspohn RB, Gösele U, San Román J, Mijangos C and Steinhart M. 2010 *Journal of Materials Chemistry* **20** 3171-7.
[11] Norman J and Desai T. 2006 *Annals of Biomedical Engineering* **34** 89-101.
[12] Ferraz N, Carlsson J, Hong J and Ott M. 2008 *Journal of Materials Science: Materials in Medicine* **19** 3115-21.
[13] Masuda H and Fukuda K. 1995 June 9, 1995 *Science* **268** 1466-8.
[14] Jessensky O, Muller F and Gosele U. 1998 *Appl Phys Lett* **72** 1173-5.
[15] Martín J, Manzano CV and Martín-González M. *Microporous and Mesoporous Materials*.
[16] Olson DA, Chen L and Hillmyer MA. 2007 2008/02/01 *Chemistry of Materials* **20** 869-90.
[17] Chen X, Chen Z, Fu N, Lu G and Yang B. 2003 *Advanced Materials* **15** 1413-7.
[18] Yanagishita T, Nishio K and Masuda H. 2006 *Japanese Journal of Applied Physics* **45**.
[19] Buyukserin F, Kang M and Martin CR. 2007 *Small* **3** 106-10.
[20] Guo LJ. 2004 *Journal of Physics D: Applied Physics* **37** R123.
[21] Cannon DM, Flachsbart BR, Shannon MA, Sweedler JV and Bohn PW. Fabrication of single nanofluidic channels in poly(methylmethacrylate) films via focused-ion beam milling for use as molecular gates: AIP; 2004.
[22] Grimm S, Giesa R, Sklarek K, Langner A, Gösele U, Schmidt H-W and Steinhart M. 2008 *Nano Letters* **8** 1954-9.
[23] Grimm S, Schwirn K, Göring P, Knoll H, Miclea Paul T, Greiner A, Wendorff Joachim H, Wehrspohn Ralf B, Gösele U and Steinhart M. 2007 *Small* **3** 993-1000.
[24] Khedkar J, Negulescu I and Meletis EI. 2002 *Wear* **252** 361-9.
[25] Ainslie KM, Bachelder EM, Borkar S, Zahr AS, Sen A, Badding JV and Pishko MV. 2006 *Langmuir* **23** 747-54.
[26] Jucius D, Grigaliunas V, Mikolajunas M, Guobiene A, Kopustinskas V, Gudonyte A and Narmontas P. *Applied Surface Science* **257** 2353-60.
[27] Baker Jr BB and Kasprzak DJ. 1993 *Polymer Degradation and Stability* **42** 181-8.
[28] Cox JM, Wright BA and Wright WW. 1964 *Journal of Applied Polymer Science* **8** 2951-61.

[29] Conesa JA and Font R. 2001 *Polymer Engineering & Science* **41** 2137-47.
[30] Fukutake N, Miyoshi N, Takasawa Y, Urakawa T, Gowa T, Okamoto K, Oshima A, Tagawa S and Washio M. *Japanese Journal of Applied Physics* **49**.
[31] Steinhart M, Wehrspohn RB, Gösele U and Wendorff JH. 2004 *Angewandte Chemie International Edition* **43** 1334-44.
[32] Steinhart M, Wendorff JH and Wehrspohn RB. 2003 *ChemPhysChem* **4** 1171-6.
[33] Young T. 1805 January 1, 1805 *Philosophical Transactions of the Royal Society of London* **95** 65-87.
[34] Liu H, Zhai J and Jiang L. 2006 *Soft Matter* **2** 811-21.
[35] Wenzel RN. 1936 1936/08/01 *Industrial & Engineering Chemistry* **28** 988-94.
[36] Cassie ABD and Baxter S. 1944 *Transactions of the Faraday Society* **40** 546-51.
[37] Sun C, Luo J, Wu L and Zhang J. 2010 *ACS Applied Materials & Interfaces* **2** 1299-302.
[38] Steinhart M, Wendorff JH, Greiner A, Wehrspohn RB, Nielsch K, Schilling J, Choi J and Gösele U. 2002 June 14, 2002 *Science* **296** 1997.
[39] Moon SI and McCarthy TJ. 2003 *Macromolecules* **36** 4253-5.
[40] Martín J and Mijangos C. 2008 *Langmuir* **25** 1181-7.
[41] Martín J, Maiz J, Sacristan J and Mijangos C. 2012 *Polymer* **53** 1149-66.
[42] Kim D, Hwang W, Park HC and Lee KH. 2008 *Current Applied Physics* **8** 770-3.
[43] Schmid G, Levering M and Sawitowski T. 2007 *Zeitschrift für anorganische und allgemeine Chemie* **633** 2147-53.
[44] Jung YC and Bhushan B. 2006 *Nanotechnology* **17** 4970.
[45] Kim D and Hwang W. 2008 *Journal of Micromechanics and Microengineering* **20** 027002.
[46] González-Rovira L, López-Haro M, Hungría AB, El Amrani K, Sánchez-Amaya JM, Calvino JJ and Botana FJ. 2010 *Corrosion Science* **52** 3763-73.
[47] Dean JA. Lange's Handbook of Chemistry. 5 ed. New York: McGraw-Hill; 1999.
[48] Bening RC and McCarthy TJ. 1990 1990/05/01 *Macromolecules* **23** 2648-55.
[49] Chakrabarti N and Jacobus J. 1988 1988/10/01 *Macromolecules* **21** 3011-4.
[50] Costello CA and McCarthy TJ. 1984 1984/12/01 *Macromolecules* **17** 2940-2.
[51] Wang S, Li J, Suo J and Luo T. 2010 *Applied Surface Science* **256** 2293-8.